Plasmon Coupled Colloidal Gold Nanorods for Near-Infrared and Short-Wave-Infrared Broadband Photodetection

Hengyang Xiang, Zhelu Hu, Chenghao Xin, Hung-ju Lin, Lionel Aigouy, Zhuoying Chen, Lei Zhou, Xiaojiao Yuan

Plasmon Coupled Colloidal Gold Nanorods for Near-Infrared and Short-Wave-Infrared Broadband Photodetection

Hengyang Xiang,[a] Zhelu Hu,[b] Chenghao Xin,[b] Hung-Ju Lin,[b]* Lionel Aigouy,[b]

Zhuoying Chen[b]*, Lei Zhou,[c] and Xiaojiao Yuan[d]*

[a] MIIT Key Laboratory of Advanced Display Materials and Devices, Institute of Optoelectronics & Nanomaterials, College of Materials Science and Engineering, Nanjing University of Science and Technology, Nanjing 210094, China.

[b] LPEM, ESPCI Paris, PSL Research University, Sorbonne Université, CNRS, 10 Rue Vauquelin, F-75005 Paris, France.

[c] Faculty of Mathematics and Physics, Huaiyin Institute of Technology, Huai'an 223003, China.

[d] Institut de Chimie Physique, UMR 8000 CNRS, Université Paris-Saclay, 91405 Orsay, France.

* Corresponding authors: E-mail: hungju95@gmail.com; zhuoying.chen@espci.fr; xiaojiao.yuan@universite-paris-saclay.fr.

Abstract

Solution-processed plasmonic colloidal gold nanorods (Au NRs) are promising candidates leading to new photodetection applications. While plasmonic Au NRs of a specific dimension will lead to a well-defined optical extinction due to the localized surface plasmon resonance, in photodetection applications broadband functioning is often desired. In this work, we achieved a broadband optical extinction from λ = 400 nm to 2000 nm by coupling colloidal Au NRs of various dimensions in a thin film form. Such an Au NR thin film was further applied on a platinum (Pt) electrode to fabricate hybrid Au-NR/Pt photodetectors. On these hybrid Au-NRs/Pt devices,

thanks to the plasmonic-induced photothermal effect, a clear broadband photoresponse was demonstrated covering the near-infrared (NIR) and short-wave-infrared (SWIR) spectrum from λ = 800 nm to 2000 nm, with a < 200 μs fast photoresponse time. This work suggests that suitably coupled plasmonic colloidal Au NRs and their strong photothermal effect are promising strategies for the future development of low-cost and broadband NIR/SWIR photodetection.

Keywords: gold nanorod, photothermal effect, plasmon coupling, broadband photodetection

1. Introduction

In recent decades, solution-processed colloidal gold nanoparticles, especially gold nanorods (Au NRs), have aroused extensive interest in the application of photo-sensing and optoelectronic devices owing to their attractive properties: (i) the dominant optical properties of surface plasmon resonance (SPR), (ii) the tunability of the nanorod aspect-ratio and the resultant tunable optical extinction, (iii) high physical & chemical stability and low biological toxicity.[1–6] Due to these fascinating properties, a great deal of research and literature have emerged on Au NRs synthesis,[7–9] self-assembling,[10–12] light scattering,[13,14] photoluminescence,[15,16] coupling modes[17–19]. Meanwhile, vast amounts of applications of colloidal Au NRs emerged in photocatalysis,[20,21] in photovoltaics,[22] in photodetectors,[23–26] and in biomedical fields (such as vivo imaging[27–29] and photothermal cancer therapy).[30–33] In particular, while isolated Au NRs of a uniform dimension typically lead to a narrow and well-defined optical extinction due to the localized surface plasmon resonance, plasmon coupled between Au NRs, arranged in proximity, can offer a possibility for broadband optical extinction. Previous studies have shown that plasmon resonances could be modified when Au NRs are close to each other either within a few nanometers or even in mechanical contact.[34] For example, P. Pramod. *et al* linked Au NRs with an

average aspect ratio of 2.7 by end-to-end assembly. They found that the extinction spectral peak has changed significantly from 600 nm to 900 nm, together with an extinction redshift caused by the plasmon coupling between Au NR dimers.[19] F. Alison M. *et al* studied Au NR trimers with the NRs arranged in various configurations. The plasmon coupling in these Au NR trimers led to a large redshift and different new extinction peaks between 700 nm and 900 nm whereas the uncoupled plasmon resonance of a single Au NR is between 624 and 678nm.[17]

While many developments in material synthesis and the optical effect due to plasmon coupling have been reported as mentioned above, the applications for broadband photon harvesting using colloidal Au NRs are still rare. J. Hao. *et al* applied a mixture of different types of Au nanoparticles to enhance the power conversion efficiency of organic solar cells aiming for an induced broadband extinction from 400 nm to 1000 nm. Such broadband extinction is caused by the different geometries of Au nanoparticles (including bone-like, rod, cube, and irregular sphere shapes).[35] On photodetection, Au NRs have been proved to be a promising medium due to their remarkable fast plasmonic-induced photothermal effect.[36,37] On this aspect, SWIR photodetectors based on a single type of Au-NRs have been demonstrated by depositing Au NRs on a 2μm by 10μm platinum short microwire.[38] To our best knowledge, broadband photodetection achieved by plasmon coupled colloidal Au NRs of different dimensions has not been demonstrated. In this paper, we investigate the plasmon coupling modes of colloidal Au NRs of different dimensions with different physical arrangements and the effect of broadband plasmon resonance in photodetection. Specifically, by combining Au NRs of different aspect ratio (AR) corresponding to various plasmon coupling modes, we have successfully obtained solution-processed Au NR films with a broadband photon harvest from 400 nm to 2000 nm. We then applied these Au NRs films for NIR and

SWIR photodetection, a spectrum window where current technologies heavily rely on the costly compound semiconductors, such as epitaxially-grown InGaAs. Hybrid Au-NR/Pt photodetectors were then realized based on plasmon-coupled Au NRs films, showing a fast photoresponse time of ~ 180 μs and a remarkable broadband photoresponse covering the NIR and SWIR spectrum window from λ = 800 nm to 2000 nm. This work proposes a bright path for broadband photodetection based on colloidal plasmonic nanoparticles, especially for the SWIR spectrum with a wavelength longer than 1000 nm where current technologies involve costly components and highly toxic elements.

2. Experimental Section

2.1 Au-NRs synthesis, Au-NR/Pt hybrid device fabrication and measurements

The synthesis procedure for colloidal Au NRs of different dimensions was described in the supporting information. To fabricate the hybrid Au-NR/Pt device, three different batches of Au NRs, namely NR750, NR980 and NR1150, were mixed together in solution according to an optimized concentration ratio of NR750: NR980: NR1150 = 1: 1: 2. The optimization strategy refers to adjusting the content of the three Au NRs in a mixed Au NR solution. The optimized concentration should give a balanced optical extinction strength, which is contributed by the three Au NRs, respectively. The optimization process is shown in Fig. S1. This mixed Au NR solution was then drop-cast and allowed to dried naturally (room temperature) onto a Pt electrode which was patterned previously onto a glass substrate by laser writing lithography (Details on the fabrication steps can be found in the supporting information). To verify the broadband photoresponsivity of this device, a monochromatic light source with a wavelength adjustable from 700 nm to 2000 nm was illuminated onto this device while resistance change (ΔR) was measured from collecting the current in the circuit with an applied DC voltage

of 2 V. The current change and ΔR was measured by both a Keithley 2634B source-measurement unit (SMU) and a Tektronix DPO2024B oscilloscope for double check. The modulation frequency for this measurement was set as 100 Hz by a mechanical chopper (SR540). The area of the light spot generated by the monochromator was measured to be about 2 mm^2, measured by an IR card (Infrared display card), which can convert the IR to visible red color. The area of the light spot at the different wavelengths used here and generated by the same monochromator was measured to be approximately the same. The power density of each wavelength was calibrated by NIST-calibrated Si and Ge photodetector. To characterize the photoresponse characteristics, a Fabry-Perot pigtailed laser (peak = 1.5 μm) was focused onto the Au-NRs/Pt device in the above circuit. The area of the laser spot is about 0.8 mm^2. The device was measured by both a Keithley 2634B SMU and a Tektronix DPO2024B oscilloscope to obtain the current change and therefore ΔR. To measure the response speed of the device at different illumination modulation frequencies (from 100 Hz to 100 kHz), the device was connected to a square-wave function generator (Agilent 33220A).

2.2 FDTD simulation

To simulate the plasmon coupling in the Au NRs of this work in different arrangement modes (M1- M6), their absorption cross-sections were calculated by finite difference time domain (FDTD) method using Lumerical commercial software. In the calculations, the Au NRs were placed on a SiO_2 substrate with different arrangement modes. The incident light source was applied by a polychromatic plane wave covering wavelengths from 500 nm to 2000 nm. For the simulation region, we applied a space-mesh size of 1 nm to balance our calculation time and geometry description of these Au NRs.

3. Results and discussions

Au NRs with different aspect ratios (ARs) of 3.7, 5.5 and 7.2 were synthesized according to previous reports[7,36] and named as NR750, NR980 and NR1150, respectively. The optical property and morphology of these Au NRs are shown in Fig. 1a-1c. The optical extinction spectra show that Au NRs can generate narrowband localized surface plasmon resonances at wavelengths of around 750 nm, 980 nm and 1150 nm, respectively. Then these three Au NR aqueous solutions were mixed in an optimized ratio of 1: 1: 2, namely, the Au-NRs-mixed solution (the black line in Fig. 1d and the red line in Fig. S1). This Au-NRs-mixed solution exhibits three optical extinction peaks ranging from 600 nm to 1400 nm as shown in Fig. 1a-1c. The extinction from 600 nm to 900 nm originates from the extinction of NR750, while the extinction from 900 nm to 1100 nm and the extinction from 1100 nm to 1400 nm is dominated by the extinction of NR980 and NR1150, respectively (Fig. 1d, black line). For diluted Au NRs dispersed in water, Au NRs are randomly and homogenously distributed inside the solution with negligible coupling between each NR, which can be verified by the TEM image in Fig. 1d. When this Au-NRs-mixed solution was drop-coated onto a glass substrate, a uniform Au NRs film was formed as shown in Fig. S2. On this Au-NRs-mixed film, a wider broadband plasmon resonance from 400 nm to 2000 nm was confirmed in the extinction spectrum (Fig. 1d, red line). Comparing the extinction spectrum of the Au-NRs-mixed solution to the one from Au-NRs-mixed film, we can observe a redshift and broadening in the extinction when Au-NRs were in film likely due to the plasmon coupling between these Au NRs. This observation originates from the reduced volume allowed for the Au NRs when they are deposited on a substrate and when the solvent dries out. It is justified that the plasmon coupling in Au-NRs-mixed film happened not only between the same Au NRs but also the ones with different sizes when comparing extinction spectrum with that of NR750, NR980 and NR1150 on glass (Fig. S3a). Comparing with the Au NRs in water solution, these Au NRs on glass substrate can be very close

with each other, even in mechanical contact, which usually will modify the plasmon resonance and give strong plasmon coupling. As visualized from the Fig. S2b, a densely packed Au NRs are resulted on the substrate, leading to plasmon coupling and a broadband optical extinction from 400 nm to 2000 nm (Fig. 1d, red line).

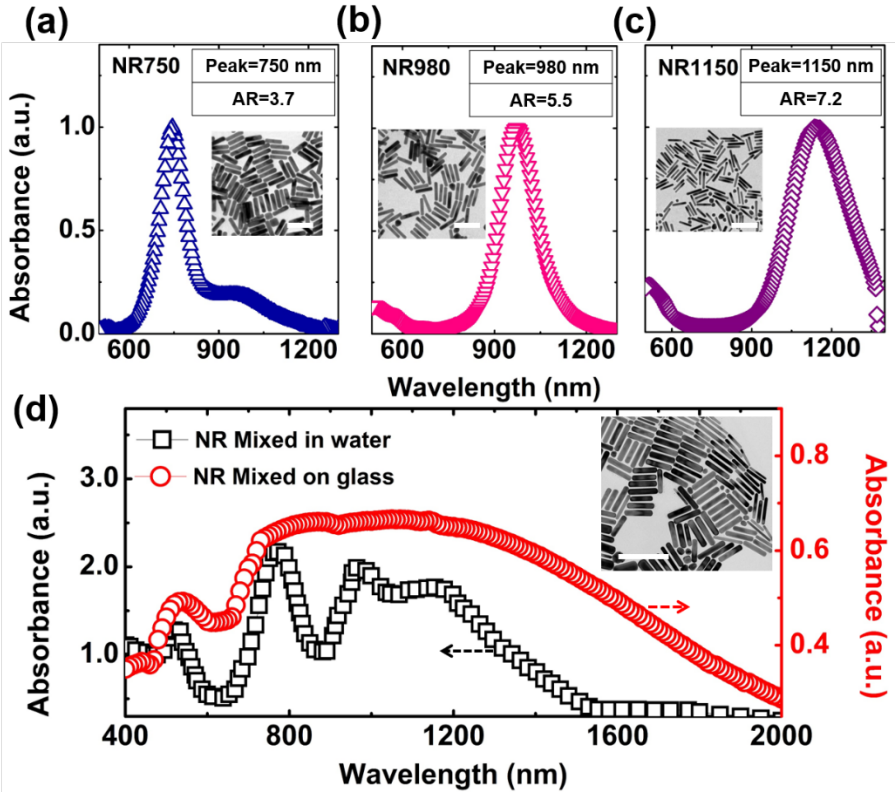

Fig. 1. Extinction spectrum of NR750 (a), NR980 (b) and NR1150 (c), their morphology is shown in the insert transmission electron microscopy (TEM) images. AR = aspect ratio. The synthesis details and the length/diameter of these Au NRs were shown in Supporting Information (Synthesis procedure and Table S1). (d) Extinction spectrum of the Au-NRs-mixed solution in water (black squares) and the extinction spectrum when this solution was deposited and dried on glass (red dots). The morphology of Au-NRs-mixed film is shown in the insert TEM image. The scale bar is 200 nm.

To understand the effect of plasmon coupling on the resultant broadband extinction spectrum, finite difference time domain (FDTD) method was applied

to calculate the absorbance changes of Au NRs when arranged in different situations. The FDTD simulations were performed using a Lumerical commercial software.[39] For simplifying the complex configurations, several possible arrangement modes (M1-M7) were built on three different sizes of Au NRs (NR750, NR980 and NR1150), as shown in Fig. 2a. Two or multiple ones were set for comparisons in different orientations by NR750, NR980 and NR1150, which were designed to calculate the plasmon coupling between Au NRs. In M1, M5 and M7, different arrangements were composed of NR750/NR980/NR1150. Arrangements with several Au NRs of the same dimension were also designed as shown in M2, M3, M4 and M6 in Fig. 2a. These Au NRs were placed on a glass (SiO_2) substrate. In our simulation, a polychromatic plane wave (500 nm - 2000 nm) was used as the incident source. The polarization of the plane wave was horizontal to the plane where these Au NRs were arranged together. For example, in the case of M1 in Fig. 2a, the polarization direction is parallel to the long axis of the Au NRs. The simulated absorption cross-section spectra of these modes were shown in Fig. 2b. These modes exhibited multiple different extinction peaks from 700 nm to 1700 nm, while these Au NRs in isolated situation (i.e. solution) showed a narrow peak at 750 nm, 980 nm and 1150 nm for NR750, NR980 and NR1150, respectively (Fig. 1a-1c). When a NR750, a NR980 and a NR1150 were arranged in a line with an interval of 0.5 nm (M1), a broadband extinction in both 600- 900 nm and 1500- 2000 nm was obtained by our simulation. When more Au NRs were in different arrangements to provide more coupling positions as shown in M5 and M7, a larger redshift and broadband extinction from 1000 nm to 2000 nm are expected. Not only modes with different Au NRs can produce plasmon coupling, Au NRs of the same dimension arranged in different situations can also produce plasmon coupling. This was observed from the simulation results for M2, M3, M4 and M6, which were arranged by different numbers of NR1150. When the number of Au NRs increased together with more

complexed arrangements, we expect that the extinction of the NR ensemble to redshift and broaden in the wavelength range from 800 nm to 1600 nm, such as the case of M6 and M7. Besides, when we summarize the extinction peaks of these modes, they can cover the entire spectrum from 700 to 2000 nm. These results demonstrated that the plasmon coupling between Au NRs leads to the broadband extinction spectrum observed when NRs were deposited on a substrate (Fig. 1d).

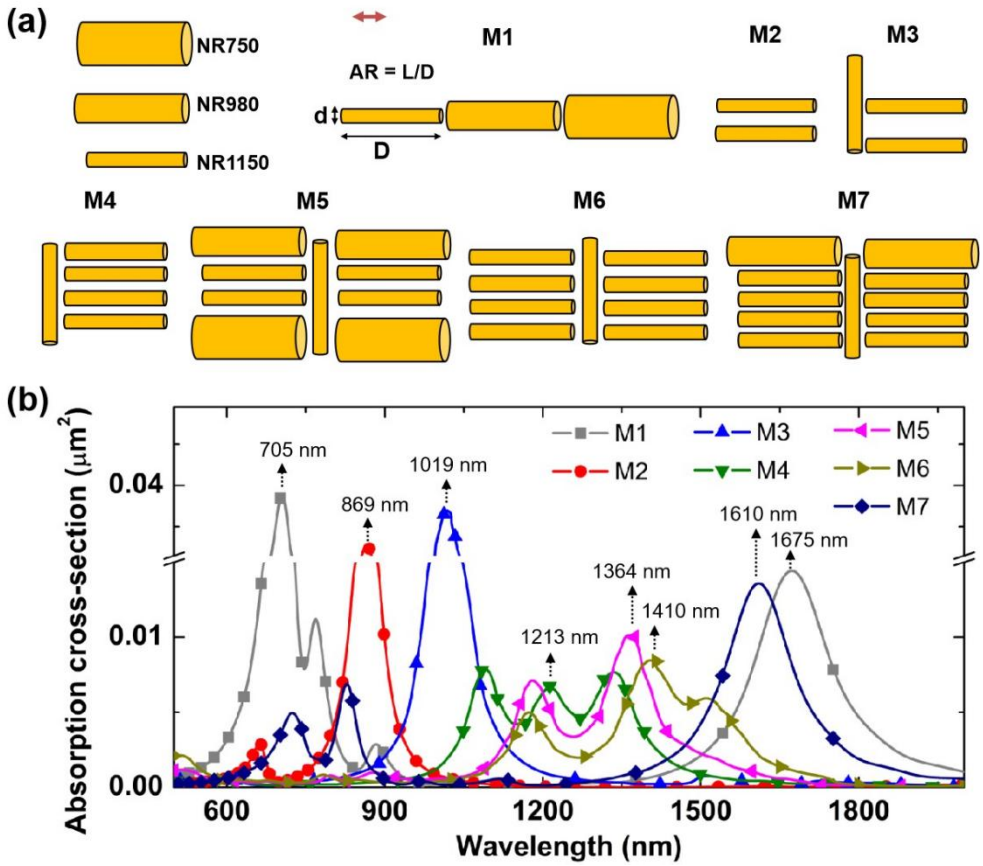

Fig. 2. (a) The Au NRs (NR750, NR980 and NR1150) were placed in different arrangement modes (M1- M7). (b) The absorption cross-section spectrum of different Au NR modes (M1- M7) simulated by finite difference time domain (FDTD). The incident polarization of the excitation light is indicated by the red arrow.

We then applied these broadband-absorbing solution-processed Au NRs films for NIR-SWIR photodetection by depositing the mixed Au NR solution on a Pt pattern (Fig. 3a). The size of this Pt pattern zone is 90 μm by 40 μm. As

revealed by SEM characterization (Fig. 3b), after drying, the mixed Au NRs were homogenously distributed on the Pt pattern. In such a hybrid Au NR/Pt device, Au NRs of different dimensions absorb photons in the NIR-SWIR spectrum and generate plasmonic-induced photothermal effect, which gives rise to a resistance change of the Pt electrode, which has a positive correlation between temperature and resistance. The Pt pattern is formed by connecting in series 11 microwires (length = 90 μm, width = 2 μm for each of them). Schematic depicting the working principle of this Au-NR/Pt photodetector is shown in the Fig. 3c. When the light is turned on, the plasmonic Au NRs absorb photons and generate heat (i.e. photothermal effect), leading to an increase of Pt resistance (step ①. Under a constant applied voltage, the current will decrease in this case (step ②). When the light turns off, the photothermal effect of Au NRs stops and heat is quickly dissipated in air and through Pt/glass substrate. Therefore, the resistance will decrease back to the room-temperature value resulting in an increased current (steps ③ and ④).

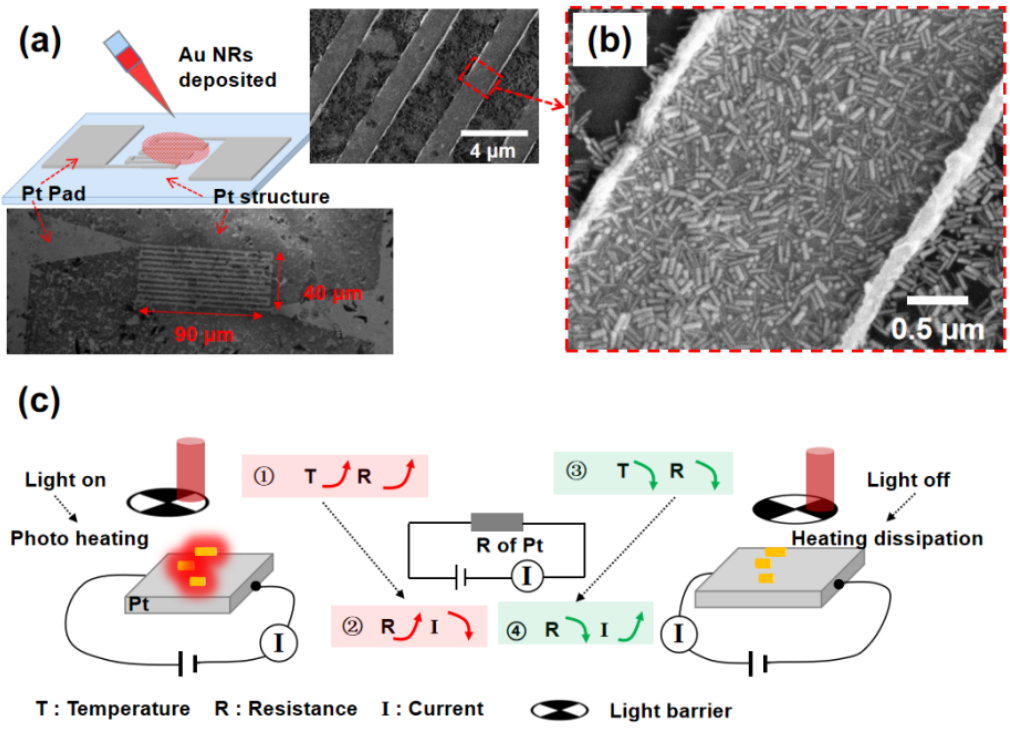

Fig. 3. (a) Device structure and size of Au-NRs/Pt photodetector. (b) Morphology of Au-NRs-mixed film drop-coated on a Pt electrode. (c) Schematic depicting the

working principle of this device as a photodetector. Step ① - ④ describes the process of the temperature (T), resistance (R), and current (I) change due to the on/off of illumination.

As mentioned above, owing to the plasmon coupling between different Au NRs in the film, broadband extinction from λ = 800 nm to 2000 nm was achieved, which should in principle allow for broadband photodetection in the NIR-SWIR range in such Au-NRs/Pt photodetectors. To demonstrate its broadband photoresponsivity, a monochromatic light source with wavelength ranging from 800 nm to 2000 nm was focused on the devices with/without Au NRs. The area of the light spot generated by the monochromator was measured to be about 2 mm^2. At a DC bias of 2 V, the change in resistance (ΔR) over time can be calculated by recording the current change in the circuit. Fig. 4a shows the photoresponse of an Au-NRs/Pt device at some wavelengths in the NIR-SWIR window from 800 nm to 2000 nm. The zoom-in photoresponse curves of two typical wavelengths (1000 nm and 1800 nm) were presented in Fig. 4b. In which, the photoresponse of control device (Pt pattern without Au NRs) at these two wavelengths was also measured. It is very obvious that the Au-NRs/Pt device achieved a remarkable photoresponse owing to the existence of Au NRs. In terms of photoresponse speed, the response time (τ, defined as the time needed for the ΔR increased from 0 to 80% of its saturated value) of this Au-NRs/Pt device at these two typical wavelengths (1000 nm and 1800 nm) can also be obtained, is around 180 μs, meaning its fast response speed in the NIR and SWIR window, as marked in Fig. 4b. The light power on the device and their power density at these wavelengths were calibrated by Si and Ge photodetector (as shown in Fig. S4). Via these measurements, the photoresponsivity in terms of resistance change rate ($RCR = (\Delta R/R_0)/P_{laser}$ in the unit of %/W) at each wavelength was summarized in Fig. 4c (black symbols). The observed broadband photoresponse from λ = 800 nm to 2000 nm resembles the measured extinction spectrum shown in Fig. 1d and the FDTD

simulation in Fig. 2b. When the responsivity was normalized and compared with single Au-NR (NR750, NR980 and NR1150) devices, it provides a wider photoresponse in NIR-SWIR range owing to these mixed Au NRs with strong plasmon coupling (Fig. S3b). In order to compare with classical photon detectors generating photocurrent under illumination, the photoresponsivity in terms of current change rate (CCR = $\Delta I/P_{laser}$ in the unit of A/W) of the current device was also measured and plotted in Fig. 4c (red symbols). Due to the correlation between ΔR and ΔI, CCR shows a similar trend consistent with RCR. The maximal photoresponsivity of the device, which is more than 13 mA/W, was observed at the wavelength of 1000 nm.

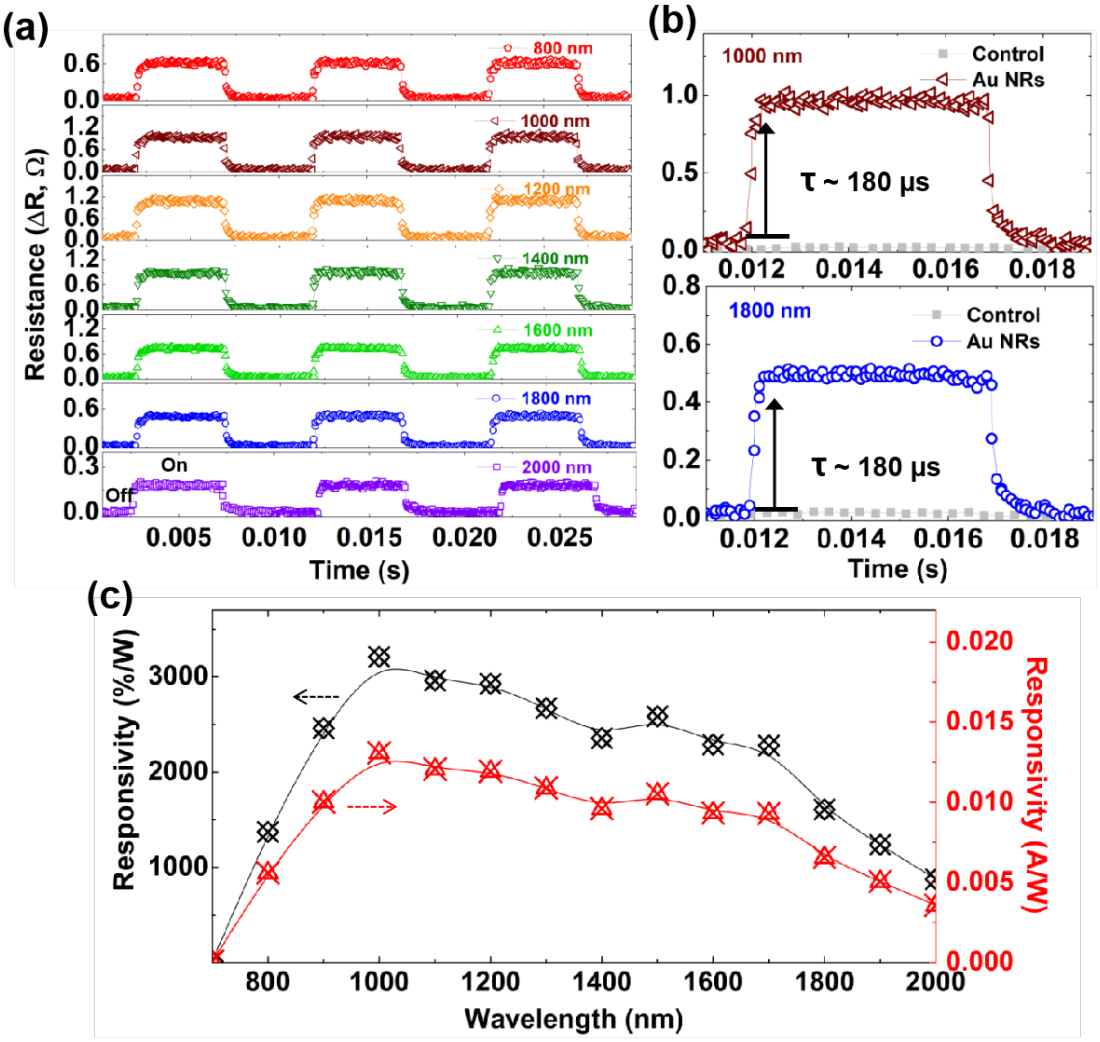

Fig. 4. (a) The photoresponse of an Au-NRs/Pt device illuminated by a monochromatic light source with a wavelength adjustable in the NIR-SWIR window from 800 nm to 2000 nm (Modulation frequency is 100 Hz). (b) Response time (τ) of this Au-NRs/Pt device at two typical wavelengths (1000 nm and 1800 nm), the grey lines are the photoresponse of control device (Pt pattern without Au NRs), showing almost no response. (c) The photoresponsivity of this Au-NRs/Pt device in the term of resistance change rate (RCR, %/W) and current change rate (CCR, A/W) in the NIR-SWIR window from 800 nm to 2000 nm. (Light power and power density at every wavelength was shown in Fig. S3).

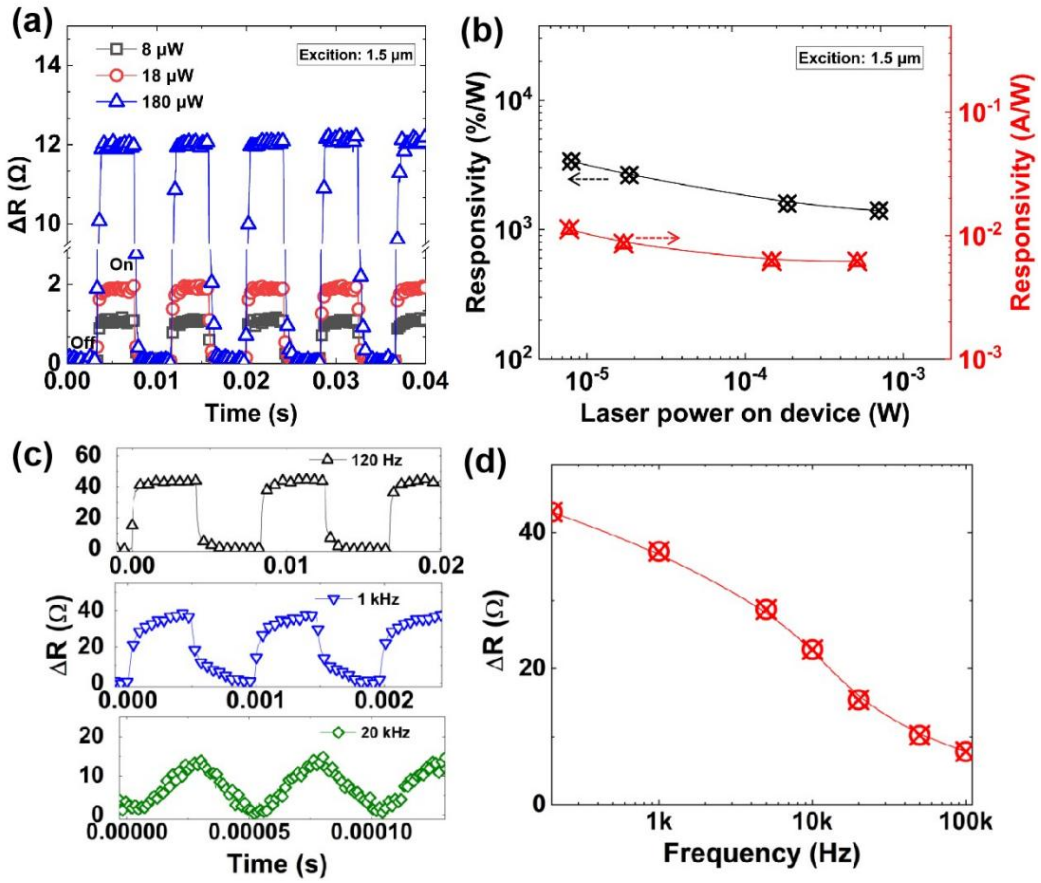

Fig. 5. (a) Resistance changes of the Au-NRs/Pt device under a 1.5 μm laser illumination with a series of laser power (8 μW, 18 μW and 180 μW, corresponding to 1 mW/cm^2, 2.25 mW/cm^2 and 22.5 mW/cm^2, respectively). (b) The photoresponsivity of this Au-NRs/Pt device in the term of resistance change rate (RCR, %/W) and current change rate (CCR, A/W) as a function of laser power changes. (c) Resistance

changes of the Au-NRs/Pt device under a 1.5 μm laser illumination modulated at the frequencies of 120 Hz, 1 kHz and 20 kHz. (d) Evolution of the resistance changes as a function of laser modulation frequency from 200 Hz to 100 kHz for the Au-NRs/Pt device.

As demonstrated in Fig. 4, this Au-NRs/Pt device possesses a remarkable photoresponsivity in the NIR-SWIR wavelength window and fast response time of ~ 180 μs at a modulation frequency of 100 Hz. Here, we continue to explore this Au-NRs/Pt device's photodetection performance under different light powers and some faster modulation frequencies. A 1.5 μm laser, as a commonly used SWIR wavelength, was used for illumination on our device with its ON/OFF modulated by a square-wave function generator with a frequency adjustable from 100 Hz to 100 kHz. The area of the laser spot was measured to be ~ 0.8 mm^2. During measurements, a DC bias of 2V was applied to the device while we measured the resistance change (ΔR) with and without illumination. As shown in Fig. 5a, clear photoresponse was observed under different laser powers under a modulation frequency of 120 Hz. The photoresponsivity of this Au-NRs/Pt device under these laser powers was also calculated out, fitting very well with the photoresponsivity obtained in Fig. 4c. Coming to response speed, when the frequency was increased, the ΔR was observed to decrease. For example, ΔR was measured to be 42 Ω at 120 Hz, which progressively decreases to 40 Ω at 1 kHz and 15 Ω at 20 kHz (Fig. 5c). Measured ΔR as a function of frequency is shown in Fig. 5d, which indicates a clear photoresponse (ΔR ≈ 8 Ω) even at a modulation frequency of 100 kHz. For this unavoidably resistance decrease trend, it can be explained by the relationship between Pt size and heat from the Au NRs. Pt pattern, as a thermistor, the ΔR depends on the amount of heat. However, in high frequency, the heat time in every cycle is shorter, the Au NRs absorb less light and therefore generate less heat, resulting in a smaller ΔR and a decreasing trend when the frequency increases.

To compare with other colloidal nanoparticle-based photodetectors, table 1 summarizes the major characteristics of colloidal plasmonic metallic nanoparticles for visible, near-IR, and/or SWIR photodetectorsn from previous applications and the current work. Despite the fact that colloidal plasmonic metallic nanoparticles, e.g. NPs[40–43] and NRs,[23,36,44] have been successfully applied previously for photodetection, in comparison to previous studies, the current results demonstrate a remarkable broadband detection covering the NIR-SWIR spectrum from λ = 800 to 2000 nm, with a detection speed comparable or faster than many previous reports. Innovations on solution-processed broadband photodetection devices in the NIR-SWIR spectrum is particularly important because current technologies detecting this spectrum window suffer from high cost and often demand highly toxic heavy metal elements. The current study thus suggests a bright path towards this goal by harnessing both the plasmon coupling of different types of colloidal Au NRs and their plasmonic-induced photothermal effect.

Table 1. Summary of applying colloidal plasmonic metallic nanoparticles for broadband photodetectors.

Materials	Peak responsivity	Response time	Response range (nm)	Ref.
Ag-NPs/CdSe-ZnS-QDs	$2.5*10^{-6}$ A/W @ 440 nm	-	400-600	[40]
Au-NRs/ZnO-nanowire	-	0.25 s	650-850	[23]
Au-NPs/TiO_2	0.5 mA/W @ 600 nm	1.5 s	400-900	[41]
SiO_2-AuNRs/SLG-InP	0.14 A/W @ 980 nm	441 ns	300-1200	[44]
Ag-PbS core-shell NPs	26.1 A/W @ 980 nm	0.17 s	370-1064	[42]

Au-PbS core-shell NPs	18.5 A/W @ 980 nm	0.32 s	405-1064	[43]
Au-NRs/NTC-thermistor	-	2.5 s	1000-1800	[36]
Au-NRs/Pt-micropattern	13 mA/W @ 1000 nm	180 μs	800-2000	**This work**

4. Conclusions

In summary, by harnessing the plasmon coupling of Au NRs of different dimensions in different configurations, broadband optical extinction was achieved in a wide visible-NIR/SWIR spectrum window from λ = 400 to 2000 nm. Applying these solution-processed plasmonic-coupled Au NRs as a nanoparticle film on a Pt electrode, Au-NR/Pt photodetectors were fabricated where we observed a fast broadband photoresponse in the NIR/SWIR spectrum window from λ = 800 nm to 2000 nm, with a photoresponse rise time of ~ 180 μs, thanks to the plasmonic-induced photothermal effect. This work proposes plasmon-coupled colloidal Au NRs and their plasmonic-induced photothermal effect as a promising strategy for the future development of low-cost, broadband and fast photodetection in the NIR and SWIR spectrum.

Conflicts of interest

There are no conflicts to declare.

Acknowledgements

This work was supported by the National Natural Science Foundation of China (62004101, 61775076), the Fundamental Research Funds for the Central Universities (30920041117), the China Postdoctoral Science Foundation (2020M681600), the Postdoctoral Research Funding Scheme of Jiangsu Province (2020Z124), the Natural Science Foundation of Jiangsu Province (BK20201476), and the Qinglan project of Jiangsu Province.

References

[1] H. Chen, L. Shao, Q. Li, J. Wang, *Chem. Soc. Rev.* **2013**, *42*, 2679.

[2] V. Sharma, K. Park, M. Srinivasarao, *Mater. Sci. Eng. R Reports* **2009**, *65*, 1.

[3] V. Amendola, R. Pilot, M. Frasconi, O. M. Maragò, M. A. Iatì, *J. Phys. Condens. Matter* **2017**, *29*, 203002.

[4] J. Cao, T. Sun, K. T. V Grattan, *Sensors Actuators B Chem.* **2014**, *195*, 332.

[5] P. Yang, J. Zheng, Y. Xu, Q. Zhang, L. Jiang, *Adv. Mater.* **2016**, *28*, 10508.

[6] Z. Cao, Z. Chen, L. Escoubas, *Opt. Mater. Express* **2014**, *4*, 2525.

[7] X. Ye, C. Zheng, J. Chen, Y. Gao, C. B. Murray, *Nano Lett.* **2013**, *13*, 765.

[8] R. Takahata, T. Tsukuda, *Chem. Lett.* **2019**, *48*, 906.

[9] K. Agrahari, R. G. Rayavarapu, *Vacuum* **2019**, *166*, 377.

[10] Z. Lu, J. Dong, Q. Han, W. Gao, Y. Wang, J. Liu, Z. Wang, Z. Sun, B. Wang, J. Qi, *J. Alloys Compd.* **2020**, *834*, 155139.

[11] X. Hu, W. Cheng, T. Wang, Y. Wang, E. Wang, S. Dong, *J. Phys. Chem. B* **2005**, *109*, 19385.

[12] C. Hamon, M. Postic, E. Mazari, T. Bizien, C. Dupuis, P. Even-Hernandez, A. Jimenez, L. Courbin, C. Gosse, F. Artzner, V. Marchi-Artzner, *ACS Nano* **2012**, *6*, 4137.

[13] H. Portalès, N. Goubet, S. Casale, X. Z. Xu, M. Ariane, A. Mermet, J. Margueritat, L. Saviot, *ACS Nano* **2020**, *14*, 4395.

[14] M.-B. Lien, J.-Y. Kim, M.-G. Han, Y.-C. Chang, Y.-C. Chang, H. J. Ferguson, Y. Zhu, A. A. Herzing, J. C. Schotland, N. A. Kotov, T. B. Norris, *ACS Nano* **2017**, *11*, 5925.

[15] B. Neupane, L. Zhao, G. Wang, *Nano Lett.* **2013**, *13*, 4087.

[16] L. Trotsiuk, A. Muravitskaya, O. Kulakovich, D. Guzatov, A. Ramanenka, Y. Kelestemur, H. V. Demir, S. Gaponenko, *Nanotechnology* **2020**, *31*, 105201.

[17] F. A. M., D. T. J., N. Carolina, M. Paul, *Philos. Trans. R. Soc. A Math. Phys. Eng. Sci.* **2011**, *369*, 3472.

[18] K. Shibata, S. Fujii, Q. Sun, A. Miura, K. Ueno, *J. Chem. Phys.* **2020**, *152*, 104706.

[19] P. Pramod, K. G. Thomas, *Adv. Mater.* **2008**, *20*, 4300.

[20] M. S. A. Che Mansor, M. N. I. Amir, N. Muhd Julkapli, A. Ma'amor, *Mater. Chem. Phys.* **2020**, *241*, 122415.

[21] H. Tian, X. Liu, Z. Liang, P. Qiu, X. Qian, H. Cui, J. Tian, *J. Colloid Interface Sci.* **2019**, *557*, 700.

[22] M. Chen, L. Shao, S. V Kershaw, H. Yu, J. Wang, A. L. Rogach, N. Zhao, *ACS Nano* **2014**, *8*, 8208.

[23] A. Pescaglini, A. Martín, D. Cammi, G. Juska, C. Ronning, E. Pelucchi, D. Iacopino, *Nano Lett.* **2014**, *14*, 6202.

[24] S. S. E. Collins, X. Wei, T. G. McKenzie, A. M. Funston, P. Mulvaney, *Nano Lett.* **2016**, *16*, 6863.

[25] W. Li, J. G. Valentine, *Nanophotonics* **2017**, *6*, 177.

[26] S. V Gaponenko, D. V Guzatov, *Proc. IEEE* **2020**, *108*, 704.

[27] Y. Tian, S. Qiang, L. Wang, *Front. Bioeng. Biotechnol.* **2019**, *7*, 398.

[28] Y. S. Chen, Y. Zhao, S. J. Yoon, S. S. Gambhir, S. Emelianov, *Nat. Nanotechnol.* **2019**, *14*, 465.

[29] C. J. Murphy, A. M. Gole, J. W. Stone, P. N. Sisco, A. M. Alkilany, E. C. Goldsmith, S. C. Baxter, *Acc. Chem. Res.* **2008**, *41*, 1721.

[30] H. Hou, L. Chen, H. He, L. Chen, Z. Zhao, Y. Jin, *J. Mater. Chem. B* **2015**, *3*, 5189.

[31] H. Deng, Y. Zhong, M. Du, Q. Liu, Z. Fan, F. Dai, X. Zhang, *Theranostics* **2014**, *4*, 904.

[32] U. Dembereldorj, S. Y. Choi, E.-O. Ganbold, N. W. Song, D. Kim, J. Choo, S. Y. Lee, S. Kim, S.-W. Joo, *Photochem. Photobiol.* **2014**, *90*, 659.

[33] S. Wang, A. Riedinger, H. Li, C. Fu, H. Liu, L. Li, T. Liu, L. Tan, M. J. Barthel, G. Pugliese, F. De Donato, M. Scotto D'Abbusco, X. Meng, L. Manna, H. Meng, T. Pellegrino, *ACS Nano* **2015**, *9*, 1788.

[34] A. M. Funston, C. Novo, T. J. Davis, P. Mulvaney, *Nano Lett.* **2009**, *9*, 1651.

[35] J. Y. Hao, Y. Xu, Y. P. Zhang, S. F. Chen, X. A. Li, L. H. Wang, W. Huang, *Chinese Phys. B* **2015**, *24*, 045201.

[36] H. Xiang, T. Niu, M. Schoenauer Sebag, Z. Hu, X. Xu, L. Billot, L. Aigouy, Z. Chen, *Small* **2018**, *14*, 1704013.

[37] H. Xiang, H.-J. Lin, T. Niu, Z. Chen, L. Aigouy, *J. Appl. Phys.* **2019**, *125*, 163101.

[38] H. Xiang, Z. Hu, L. Billot, L. Aigouy, Z. Chen, *Nanoscale* **2019**, *11*, 18124.

[39] Lumerical Inc., *Vancouver, BC V6E 2M6,* **2018**, *9*.

[40] L. Huang, C. C. Tu, L. Y. Lin, *Appl. Phys. Lett.* **2011**, *98*, 113110.

[41] C. V Hoang, K. Hayashi, Y. Ito, N. Gorai, G. Allison, X. Shi, Q. Sun, Z. Cheng, K. Ueno, K. Goda, H. Misawa, *Nat. Commun.* **2017**, *8*, 771.

[42] M. Mozafari, S. Nasresfahani, M. H. Sheikhi, H. Agharezaei, *J. Alloys Compd.* **2021**, *850*, 156831.

[43] X. Zhao, Y. Duan, K. Li, Y. Fang, X. Song, H. Zhang, H. Yu, *J. Mater. Sci.* **2019**, *54*, 14720.

[44] L. B. Luo, Y. F. Zou, C. W. Ge, K. Zheng, D. D. Wang, R. Lu, T. F. Zhang, Y. Q. Yu, Z. Y. Guo, *Adv. Opt. Mater.* **2016**, *4*, 763.